Electronic Supplementary Material (ESI) for Analytical Methods.

Supplemental Information

Effective Discrimination of Gas-Phase Peptide Conformers using TIMS-ECD-ToF MS/MS

K. Jeanne Dit Fouque,[a,b] M. Wellmann,[c] D. Leyva Bombuse,[a] M. Santos-Fernandez,[a] Y. L. Cintron-Diaz,[a] M. E. Gomez,[a] D. Kaplan,[d] V. G. Voinov,[e,f] and F. Fernandez-Lima*[a,b]

[a] *Department of Chemistry and Biochemistry, Florida International University, Miami, FL 33199, United States.*

[b] *Biomolecular Science Institute, Florida International University, Miami, FL 33199, United States.*

[c.] *Institute of Physical Chemistry, Christian-Albrechts-University Kiel, 24098 Kiel, Germany.*

[d.] *KapScience LLC, Tewksbury, MA 01876, United States.*

[e.] *e-MSion Inc., Corvallis, OR 97330, United States.*

[f.] *Linus Pauling Institute and Department of Biochemistry and Biophysics, Oregon State University, Corvallis, OR 97331, United States.*

Corresponding Author

fernandf@fiu.edu

Table of Contents:

Scheme S1. Schematic showing the Cornell and Utah–Washington mechanisms for N–Cα bond cleavage in ExD of peptides and proteins.

Figure S1. Schematic of the TIMS-q-EMS-ToF MS instrument.

Table S1. Optimized electrostatic potentials, filament current and collision energy settings in the transmission and ECD modes for the EMS cell.

Figure S2. ECD/CID spectra of the ion mobility-selected $[M + 2H]^{2+}$ ions of substance P acquired in TIMS-q-ECD/CID -ToF MS/MS and FT-ICR-ECD MS/MS platforms.

Figure S3. ECD/CID spectra of the ion mobility-selected $[M + 2H]^{2+}$ ions of AT-Hook 3 acquired in TIMS-q-ECD/CID -ToF MS/MS and FT-ICR-ECD MS/MS platforms.

Results and Discussion. Ion Mobility selected –ECD/CID MS/MS of Angiotensin I $[M + 2H]^{2+}$

Figure S4. TIMS-q-EMS-ToF and FT-ICR-ECD MS/MS analysis of angiotensin I $[M + 2H]^{2+}$ ions.

Figure S5. ECD/CID spectra of the ion mobility-selected $[M + 2H]^{2+}$ ions of angiotensin I acquired in TIMS-q-ECD/CID -ToF MS/MS and FT-ICR-ECD MS/MS platforms.

Results and Discussion. Ion Mobility selected –ECD/CID MS/MS of Bradykinin $[M + 2H]^{2+}$

Figure S6. TIMS-q-EMS-ToF and FT-ICR-ECD MS/MS analysis of bradykinin $[M + 2H]^{2+}$ ions.

Figure S7. ECD/CID spectra of the ion mobility-selected $[M + 2H]^{2+}$ ions of bradykinin acquired in TIMS-q-ECD/CID -ToF MS/MS and FT-ICR-ECD MS/MS platforms.

Figure S8. ECD spectra of the $[M + 2H]^{2+}$ ions for all investigated peptides when TIMS operations is on/off.

Table S2. ECD efficiency yields of the investigated peptides obtained in the TIMS-q-ECD-ToF MS per ion mobility band and in the FT-ICR MS platforms.

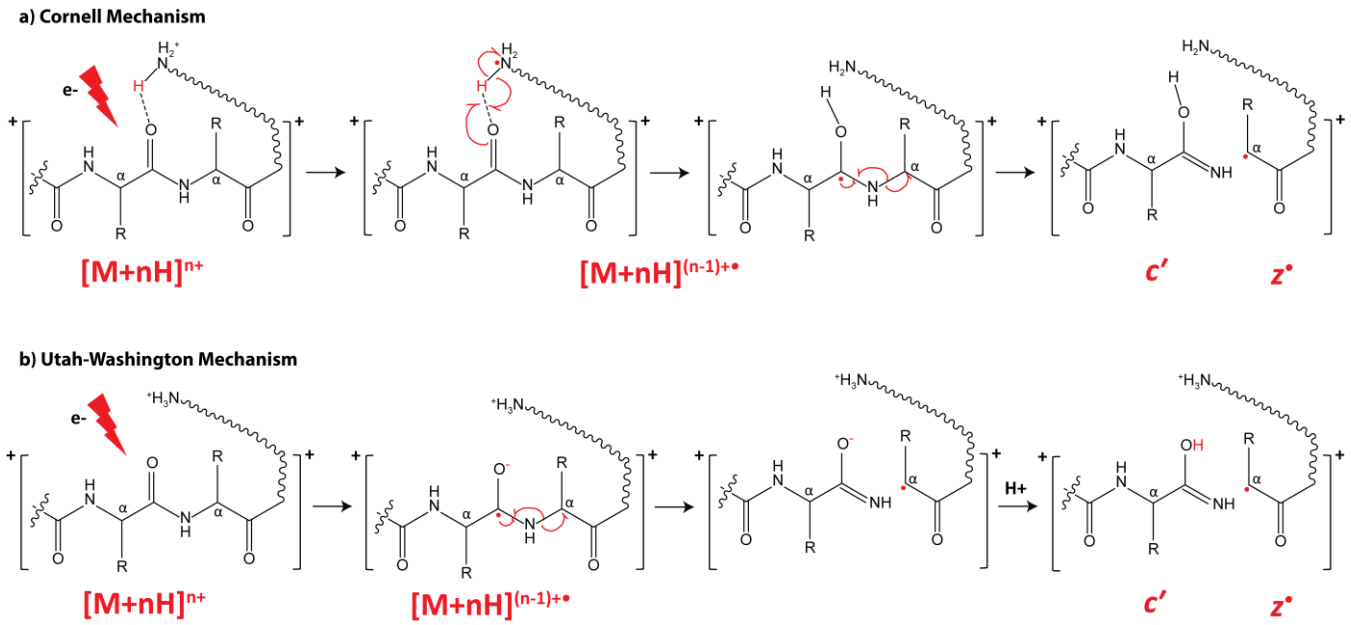

Scheme S1. Schematic showing the (a) Cornell and (b) Utah–Washington mechanisms for N–Cα bond cleavage in ExD of peptides and proteins.

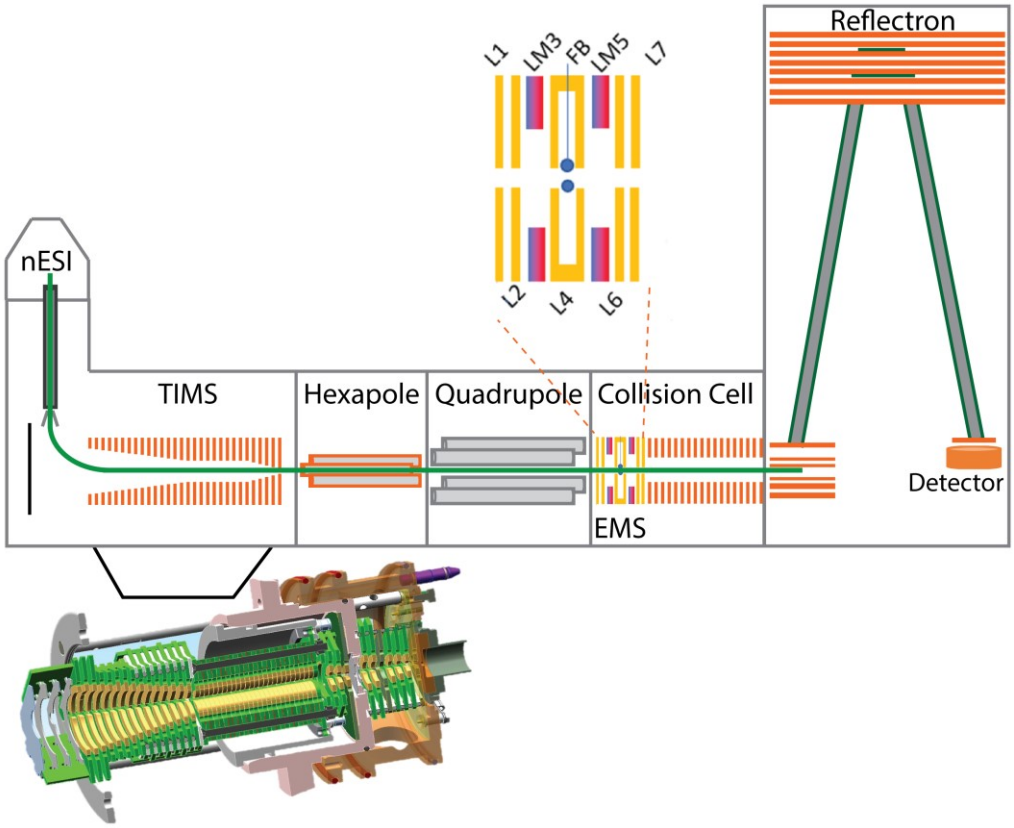

Figure S1. Schematic of the TIMS-q-EMS-ToF MS instrument. Insets illustrates the design of the convex electrode TIMS geometry as well as the EMS lenses (L1-L7), magnet (LM3 an LM5) and filament (FB) arrangement.

Table S1. Optimized electrostatic potentials, filament current and collision energy settings in the transmission and ECD modes for the EMS cell.

Parameters	Settings in Transmission Mode	Settings in ECD Mode
L1	34.5 V	27.5 V
L2	-43.8 V	36.6 V
LM3	33.2 V	44.5 V
L4	32.0 V	46.3 V
FB	31.1 V	33.5 V
LM5	30.0 V	36.1 V
L6	29.1 V	35.9 V
L7	28.3 V	29.0 V
FB current	0 A (off)	2.5 A
Collision Energy	10 eV	2 eV

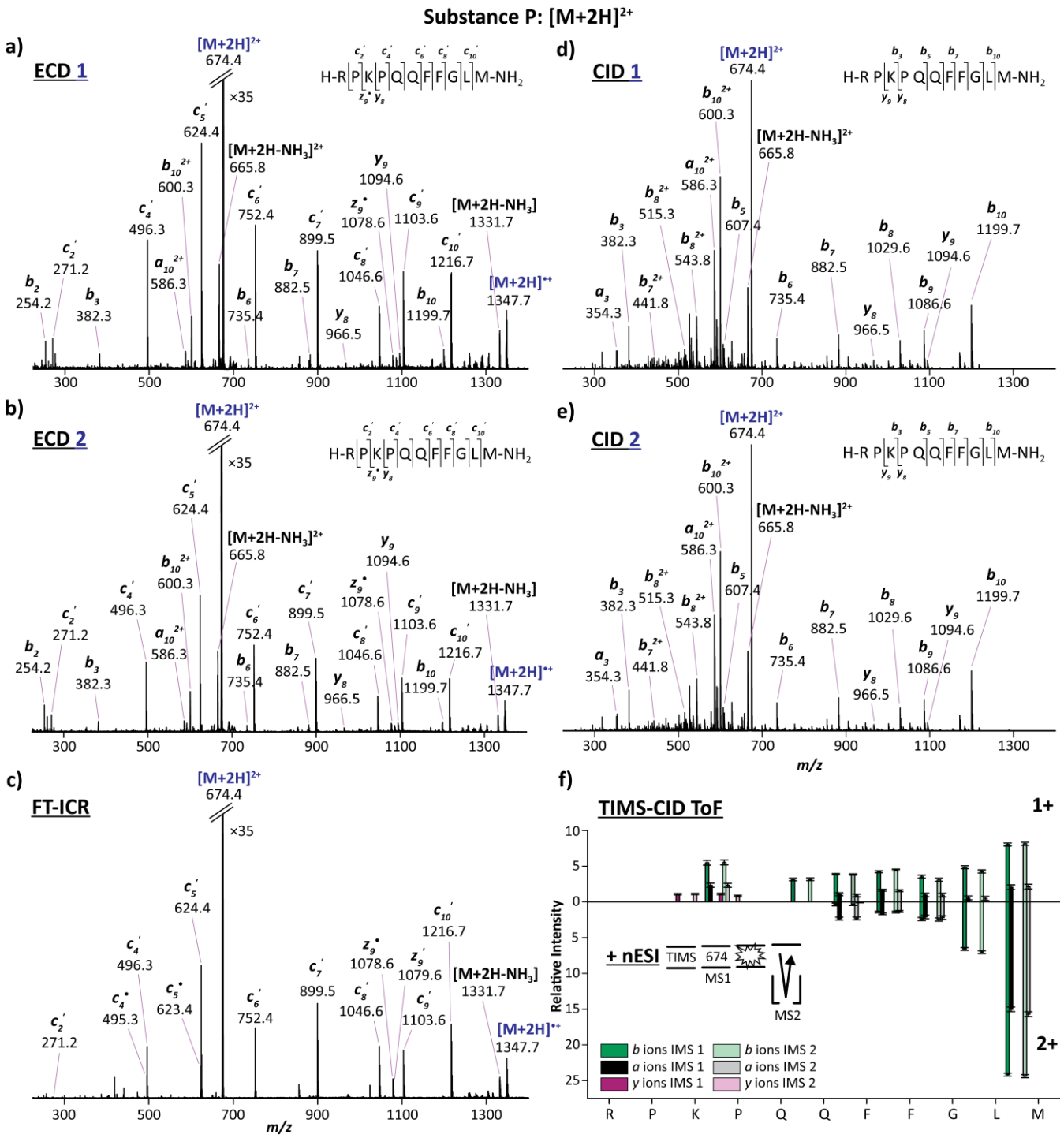

Figure S2. ECD/CID spectra of the ion mobility-selected $[M + 2H]^{2+}$ ions of substance P acquired in (a,b) TIMS-q-ECD-ToF MS/MS, (c) FT-ICR-ECD MS/MS and (d,e) TIMS-q-CID-ToF MS/MS platforms. (f) Bar plots showing the relative intensities of the CID product ions per IMS bands for the selected $[M + 2H]^{2+}$ ions.

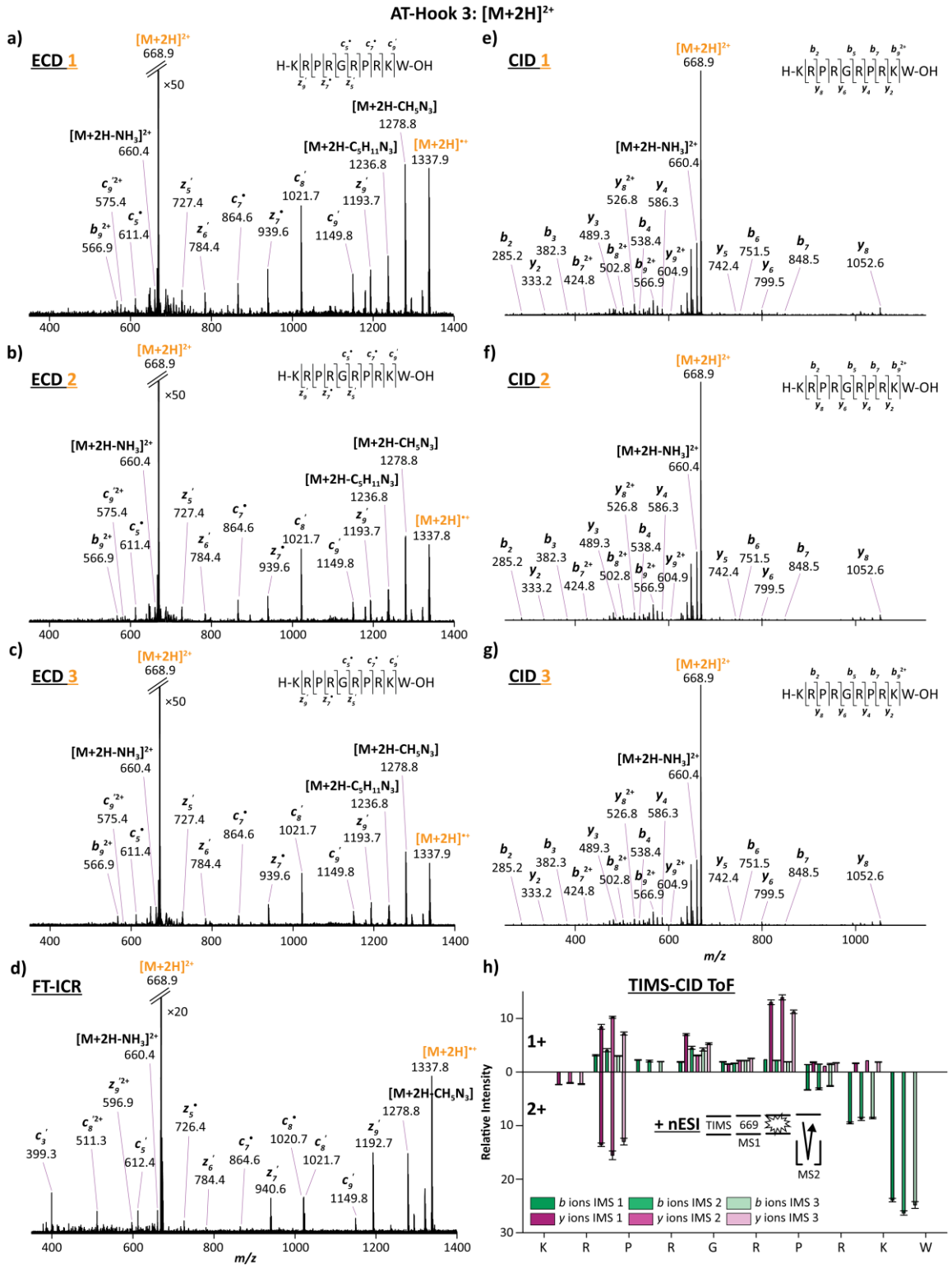

Figure S3. ECD/CID spectra of the ion mobility-selected $[M + 2H]^{2+}$ ions of AT-Hook 3 acquired in (a-c) TIMS-q-ECD-ToF MS/MS, (d) FT-ICR-ECD MS/MS and (e-g) TIMS-q-CID-ToF MS/MS platforms. (h) Bar plots showing the relative intensities of the CID product ions per IMS bands for the selected $[M + 2H]^{2+}$ ions.

Ion Mobility selected –ECD/CID MS/MS of Angiotensin I $[M + 2H]^{2+}$

Typical ion mobility, precursor ion mass and relative intensity of observed ECD fragments in TIMS-q-EMS-ToF MS/MS and FT-ICR-ECD MS/MS of the $[M + 2H]^{2+}$ angiotensin I molecular ion are shown in Figure S4. The TIMS analysis for the $[M + 2H]^{2+}$ molecular species of angiotensin I resulted in the observation of three IMS bands, separated with an apparent ion mobility $R \sim 145$ using a $Sr = 0.26$ V/ms (Figure S4a). Inspection of the ion mobility-selected ECD/CID spectra showed similar features between the IMS 1, IMS 2 and IMS 3 bands as well as the FT-ICR ECD MS/MS spectra (Figure S5). The charge-reduced $[M + 2H]^{\bullet+}$ ions (m/z 1297.7) were always observed with the largest abundance, as signature ions of the ECD events. In addition, $c_i'/z_j^{\bullet}$ series were observed, consisting of c_2' to c_9' and $z_3^{\bullet}$ to $z_9^{\bullet}$ product ions (except for c_6' and $z_4^{\bullet}$ due to Pro7, Figure S4c). In the TIMS-q-EMS-ToF MS/MS experiments, a fragmentation efficiency of ~ 0.5% relative to the intensity of the precursor ions was observed for the most abundant c_7' ECD product ions. The total ECD fragmentation efficiency obtained in the TIMS-q-EMS-ToF MS/MS platform matches that of the FT-ICR ECD MS/MS (~ 4.7% vs. ~ 3.6%, respectively, Table S2). Analogous to the case of substance P, ECD experiments of angiotensin I displayed higher extents of hydrogen migration (H• transfer) in the FT-ICR ECD MS/MS when compared to the TIMS-q-EMS-ToF MS/MS platform (Figure S4d). For example, significant H• migration was observed at Val3, Tyr4 and Ile5 residues, including $c_3^{\bullet}$, $c_4^{\bullet}$ and $c_5^{\bullet}$ as well as z_7' and z_8' fragment ions. These results suggest that the bulky Tyr4 residue of angiotensin I provides sufficient steric hindrance to be in proximity of the nearby residues, facilitating H• transfer in this region.

The ion mobility-selected ECD/CID fragmentation patterns (i.e., $c_i'/z_j^{\bullet}$ and b_i/y_j series) of angiotensin I were similar for the three IMS bands, suggesting that these IMS bands correspond to conformers that follow the same protonation scheme. The presence of c_2' to c_5' fragments for all IMS bands is consistent with Arg2 as potential protonated residue, while $z_3^{\bullet}$ with y_2 to y_4 product ions point towards the protonation of the His9 residue. Moreover, differences in the relative abundance and hydrogen exchange were observed across the ion mobility selected EMS spectra. One of the main differences was located at the Ile5 residue, for which the higher relative abundance of the b_5 product ions was observed for IMS 3 while decreasing toward the IMS band 1 (green bars in Figure S5h). This suggests that the Ile5 residue is likely more exposed and more easily accessible to cleavage when the structure is more extended. Likewise, c_3' fragments were found having higher relative abundances for IMS 1 and IMS 2 bands relative to IMS 3 band (blue bars), suggesting that Val3 residue is more exposed when the structure is compact. This analysis is consistent with the higher H• transfer in the IMS 3 band (Figure S4d) related to Val3 residue proximity to the Tyr4 sidechain, making the Val3-Tyr4 peptide bonds harder to cleave. Another difference was observed at the Pro7-Phe8 peptide bond, where differences in the H• migration event were observed. The z_3' product ions exhibited higher abundance of hydrogen migration for the IMS 3 band, indicating of Pro7 residue proximity to the Phe8 sidechain. In addition, lower abundance of b_6 fragments in IMS band 3 as compared to IMS bands 1 and 2, suggested that the His6-Pro7 peptide bond in the IMS 3 band is probably in a *cis*-configuration. The b_6 feature was also consistent with the ion mobility-selected CID experiments (Figure S5h). The lower abundance of z_3' product ions combined with the higher abundances of b_6 fragments suggested that the His6-Pro7 peptide bond is probably in a *trans*-configuration in the IMS 1 and IMS 2 bands. The c_8'/b_8 product ions were found in lower relative abundance in the IMS 3 band probably due to a *cis* configuration of the Pro7 residue that makes the cleavage between Phe8 and His9 residues less accessible.

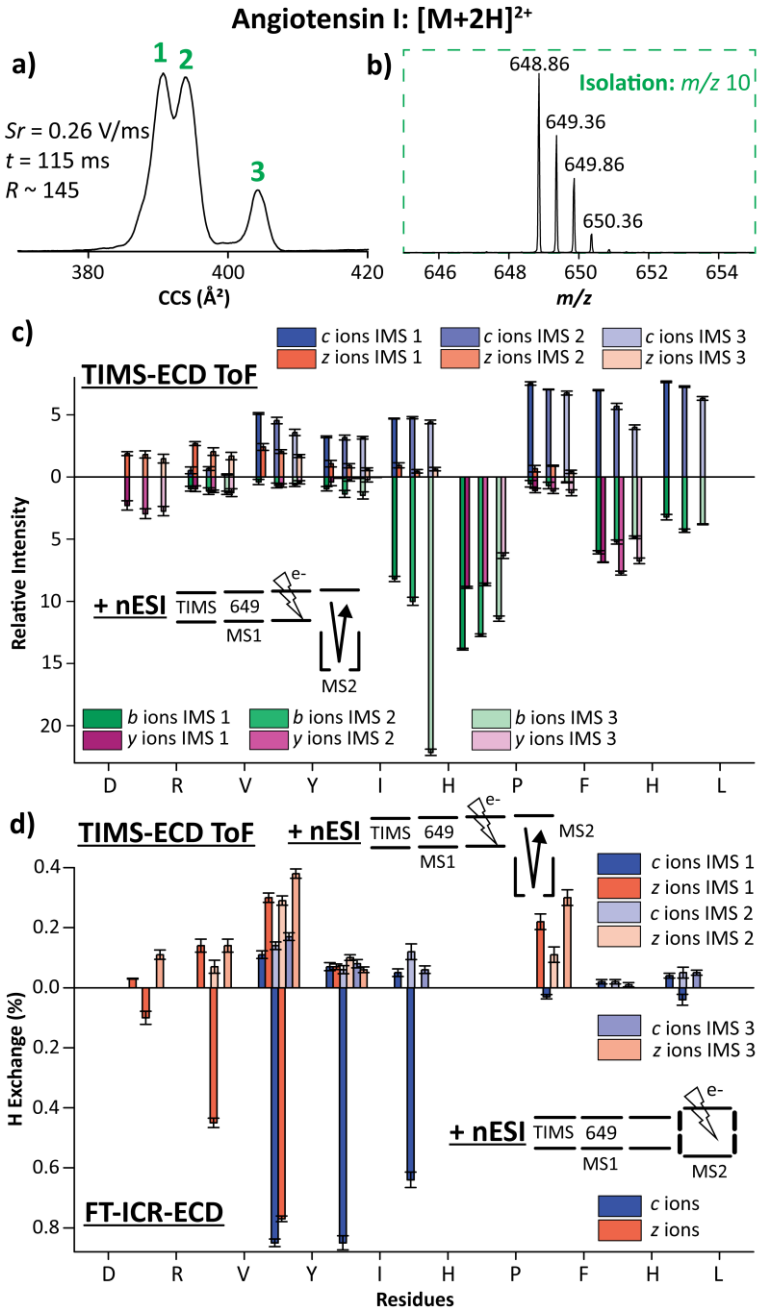

Figure S4. TIMS-q-EMS-ToF and FT-ICR-ECD MS/MS analysis of angiotensin I $[M + 2H]^{2+}$ ions (m/z 648.9). (a) Typical TIMS profiles, (b) quadrupole isolation window of the precursor ion, (c) bar plots showing the relative intensities of the ECD product ions per IMS bands for the selected $[M + 2H]^{2+}$ ions, and (d) bar plot showing the hydrogen migration events of angiotensin I observed in the two MS platforms, obtained by comparison between the experimental and theoretical isotopic patterns. Note that relative intensities were calculated using peak heights and divided by the sum of all fragments for direct comparison across IMS bands. c_i/z_j and b_i/y_j ions are plotted above and below the horizontal axis, respectively in (c). Error bars from triplicate measurements are represented on the bar plots. Ion mobility selected ECD/CID and FT-ICR ECD spectra are shown in Figure S5).

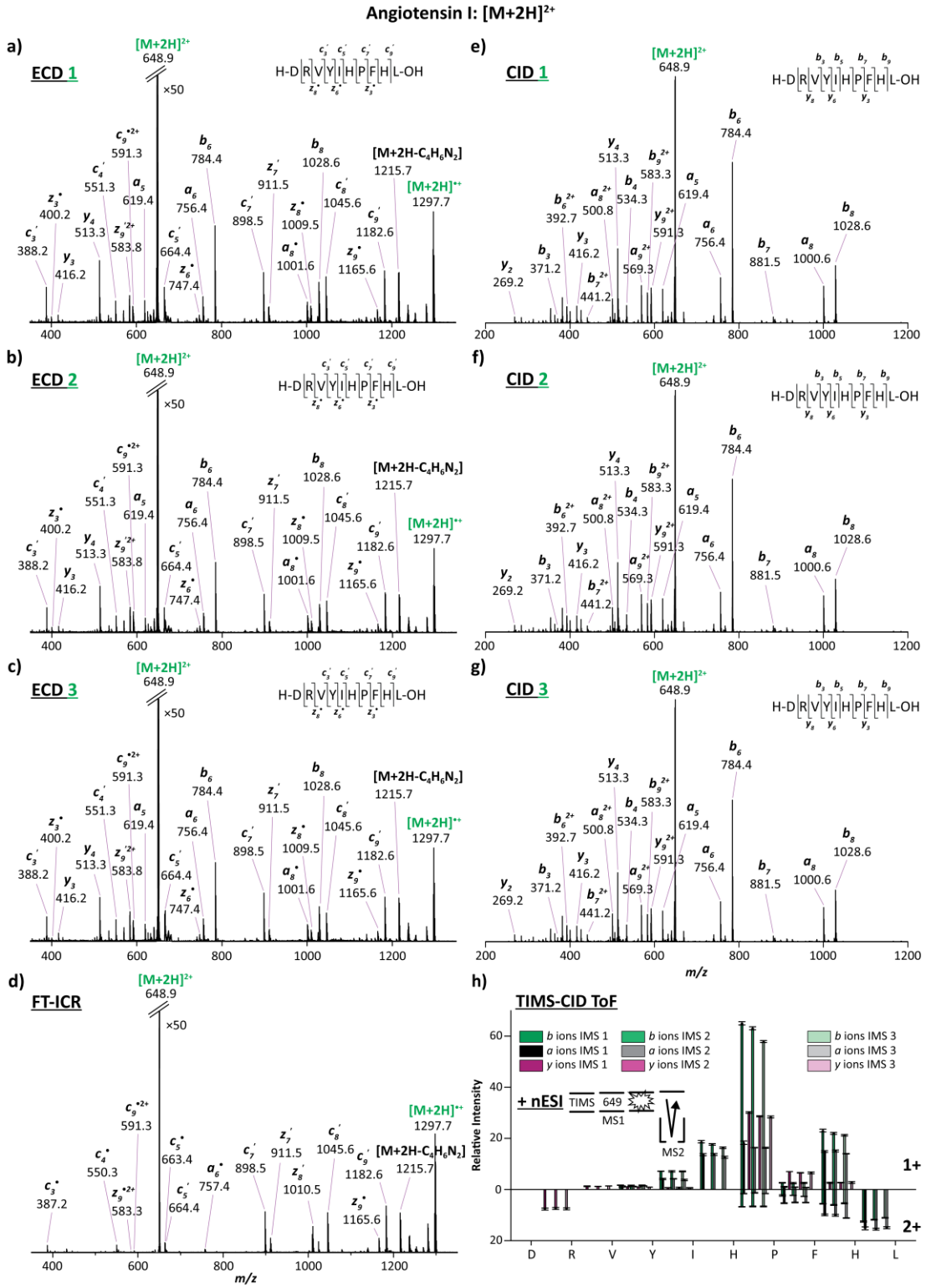

Figure S5. ECD/CID spectra of the ion mobility-selected $[M + 2H]^{2+}$ ions of angiotensin I acquired in (a-c) TIMS-q-ECD-ToF MS/MS, (d) FT-ICR-ECD MS/MS and (e-g) TIMS-q-CID-ToF MS/MS platforms. (h) Bar plots showing the relative intensities of the CID product ions per IMS bands for the selected $[M + 2H]^{2+}$ ions.

Ion Mobility selected –ECD/CID MS/MS of Bradykinin I $[M + 2H]^{2+}$

Typical ion mobility, precursor ion mass and relative intensity of observed ECD fragments in TIMS-q-EMS-ToF MS/MS and FT-ICR-ECD MS/MS of the $[M + 2H]^{2+}$ bradykinin molecular ion are shown in Figure S6. The TIMS analysis for the $[M + 2H]^{2+}$ molecular species of bradykinin resulted in the observation of three resolved IMS bands, separated with an apparent ion mobility $R \sim 120$ using a $Sr = 0.26$ V/ms (Figure S6a). Inspection of the ion mobility-selected ECD/CID spectra showed similar features between the IMS 1, IMS 2 and IMS 3 bands as well as the FT-ICR ECD MS/MS spectra (Figures S7). The charge-reduced $[M + 2H]^{\bullet+}$ ions (m/z 1060.6) were always observed, as signature ions of the ECD events. In addition, $c_i'/z_j^{\bullet}$ series were observed, consisting of c_3' to c_8' and $z_2^{\bullet}$ to $z_6^{\bullet}$ product ions (except for c_6' and $z_3^{\bullet}$ due to Pro7, Figure S6c). In the TIMS-q-EMS-ToF MS/MS experiments, a fragmentation efficiency of ~1.3% relative to the intensity of the precursor ions was observed for the most abundant c_5' ECD product ions. The total ECD fragmentation efficiency obtained in the TIMS-q-EMS-ToF MS/MS platform matches that of the FT-ICR ECD MS/MS (~ 4.8% vs. ~ 4.4%, respectively, Table S2). Hydrogen migration (H• transfer) events were found more pronounced for the FT-ICR ECD MS/MS when comparing with those obtained in the EMS cell (Figure S6d). Product ions that involve significant H• migration were observed at Pro3, Gly4 and Phe5 residues, including $c_3^{\bullet}$, $c_4^{\bullet}$ and $c_5^{\bullet}$ as well as z_4', z_5' and z_6' fragment ions. This suggests that a rigid fold may occur in the bradykinin structure induced by the two proline residues (Pro2 and Pro3). This fold may bring the nearby residues in proximity from the bulky side-chain of the Phe5 residue, facilitating the H• transfer.

The ion mobility-selected ECD/CID fragmentation patterns (i.e., $c_i'/z_j^{\bullet}$ and b_i/y_j series) of bradykinin were similar for the three IMS bands (Figures S6c and S7h), suggesting that these IMS bands correspond to conformers that follow the same protonation scheme, in good agreement with previous reports from Clemmer and co-workers.[1] In fact, the presence of c_3' to c_5' fragments for all IMS selected ECD spectra suggests that the Arg1 residue is probably protonated, while $z_2^{\bullet}$ product ions is consistent with Arg9 as potential protonated residue. No significant differences in the relative abundance and hydrogen exchange of product ions were observed across the IMS selected ECD/CID spectra in the Ser6-Arg9 region (Figures S6c and S7h). This is consistent with previous observations, for which the well-defined β-turn motif of this region is conserved, while the Arg1-Phe5 residues lead to distinct populations, including *cis*/*trans*-isomerization at Pro residues.[1,2] Moreover, the absence of significant H• transfer in the Ser6-Arg9 region suggests that the Pro7 residue is in a *trans*-configuration for all IMS bands.

Differences were observed across the IMS selected spectra in the Arg1-Phe5 region, for which the z_6' product ions exhibited significantly higher hydrogen exchange for the IMS 3 band (red bars in Figure S6d). This suggests that the Pro3 residue is probably in proximity of the Pro2 residue as well as the bulky Phe6 residue, indicating that the Pro2 and Pro3 residues might be in a *cis*-configuration for the IMS 3 band only. This feature is also consistent with the slightly lower relative intensity of the y_7 and y_8 product ions, corresponding to the Pro2-Pro3 and Arg1-Pro2 peptide bonds, respectively (purple bars in Figures S6c and S7h). In addition, the IMS 1 selected ECD spectra displayed higher z_6' fragments as compared to IMS 2 but lower than IMS 1, suggesting that the Pro3 residue is either in proximity to the Pro2 residue or the bulky Phe6 residue. This means that one of the Pro2 and Pro3 residues is probably in a *cis*-configuration for the IMS 1 band. Moreover, lower H• transfer was observed at Pro3 residue for the IMS 2 selected ECD spectra, suggesting that Pro3 residue interacts with a lesser extent with the Pro2 and Phe5 side-chains (as compared to IMS 1 and 3 bands) consistent with the Pro2 and Pro3 residues in a *trans*-configuration. In summary, the ion mobility-selected ECD fragmentation experiments suggest that the IMS 1-3 bands correspond to *trans*-Pro2/*cis*-Pro3/*trans*-Pro7 and/or *cis*-Pro2/*trans*-Pro3/*trans*-Pro7, *trans*-Pro2/*trans*-Pro3/*trans*-Pro7 and *cis*-Pro2/*cis*-Pro3/*trans*-Pro7, respectively.

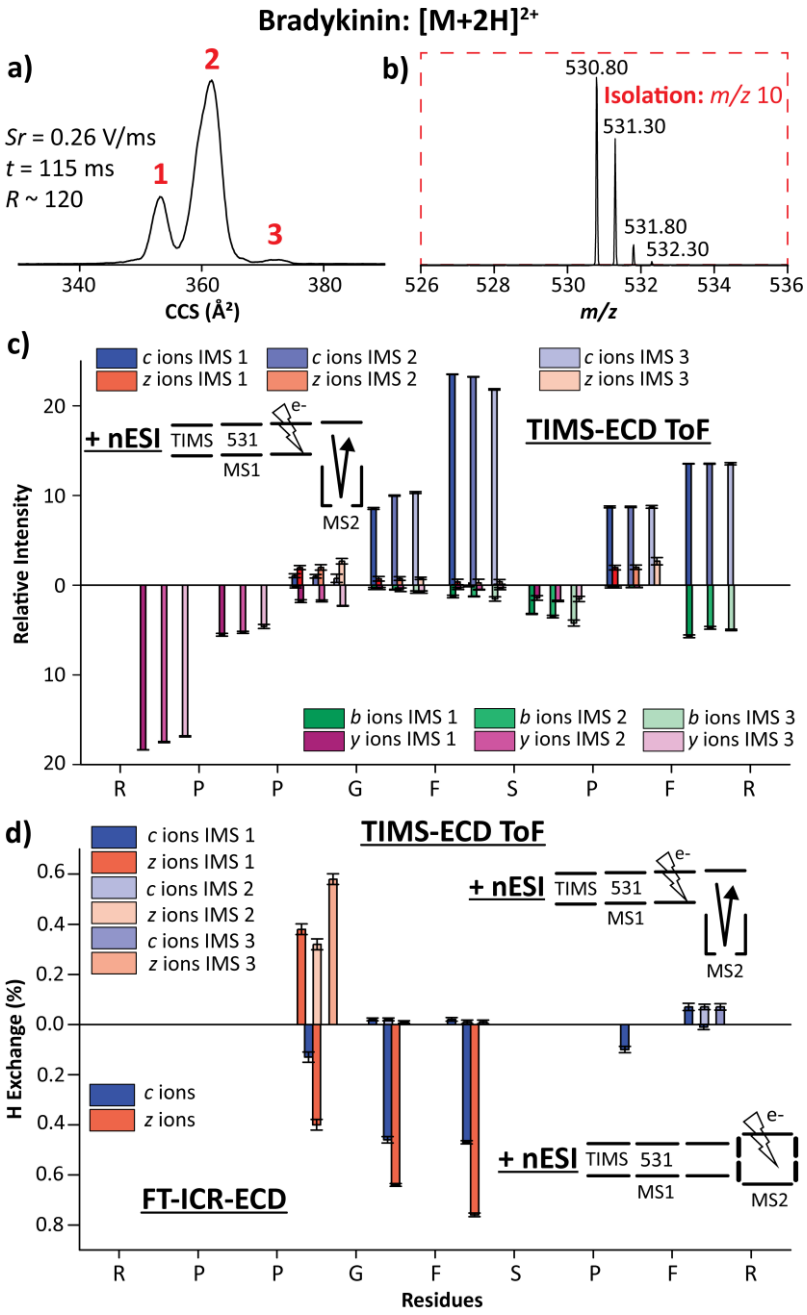

Figure S6. TIMS-q-EMS-ToF and FT-ICR-ECD MS/MS analysis of bradykinin $[M + 2H]^{2+}$ ions (m/z 530.8). (a) Typical TIMS profiles, (b) quadrupole isolation window of the precursor ion, (c) bar plots showing the relative intensities of the ECD product ions per IMS bands for the selected $[M + 2H]^{2+}$ ions, and (d) bar plot showing the hydrogen migration events of bradykinin observed in the two MS platforms, obtained by comparison between the experimental and theoretical isotopic patterns. Note that relative intensities were calculated using peak heights and divided by the sum of all fragments for direct comparison across IMS bands. c_i/z_j and b_i/y_j ions are plotted above and below the horizontal axis, respectively in (c). Error bars from triplicate measurements are represented on the bar plots. Ion mobility selected ECD/CID and FT-ICR ECD spectra are shown in Figure S7).

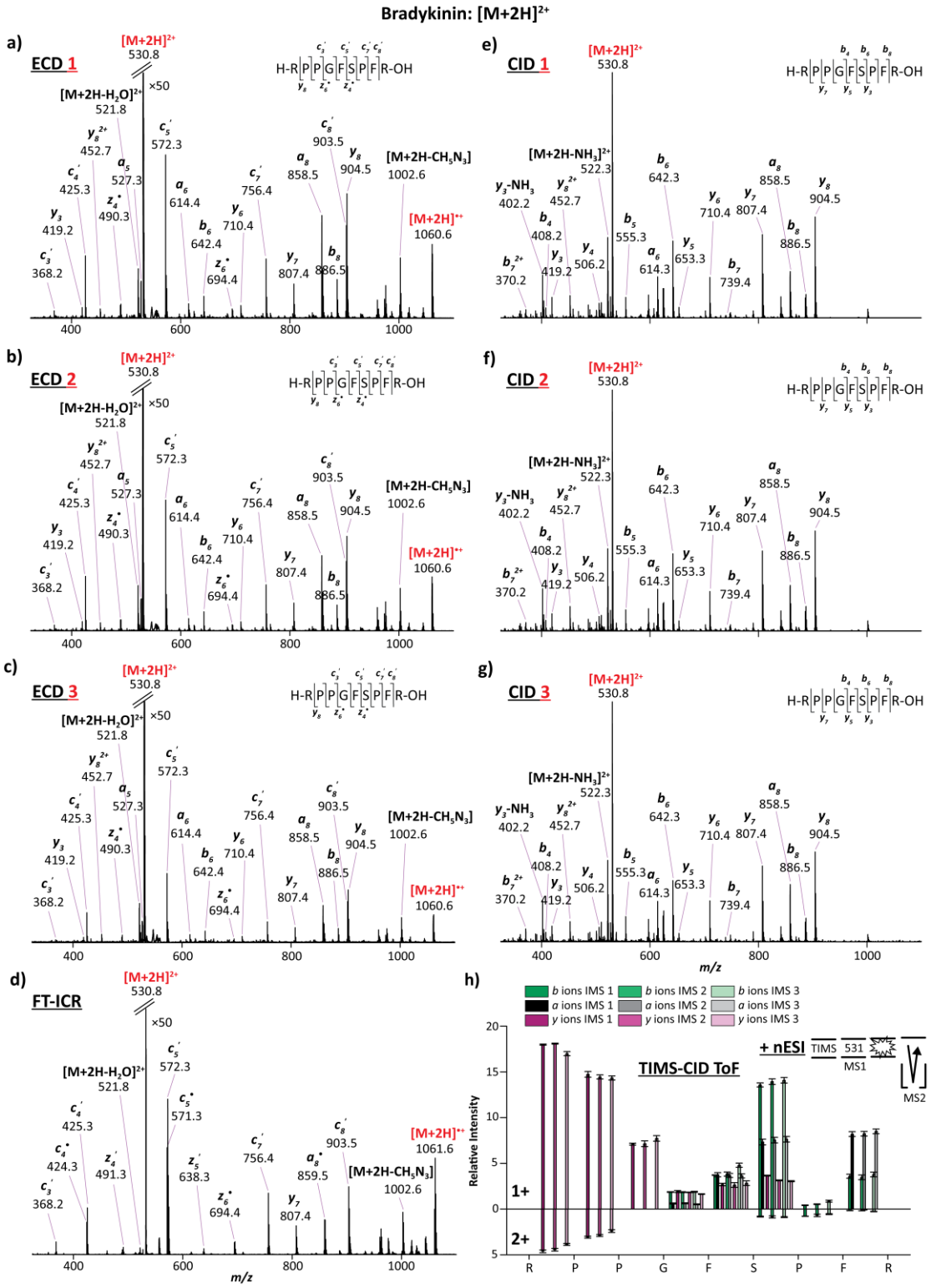

Figure S7. ECD/CID spectra of the ion mobility-selected $[M + 2H]^{2+}$ ions of bradykinin acquired in (a-c) TIMS-q-ECD-ToF MS/MS, (d) FT-ICR-ECD MS/MS and (e-g) TIMS-q-CID-ToF MS/MS platforms. (h) Bar plots showing the relative intensities of the CID product ions per IMS bands for the selected $[M + 2H]^{2+}$ ions.

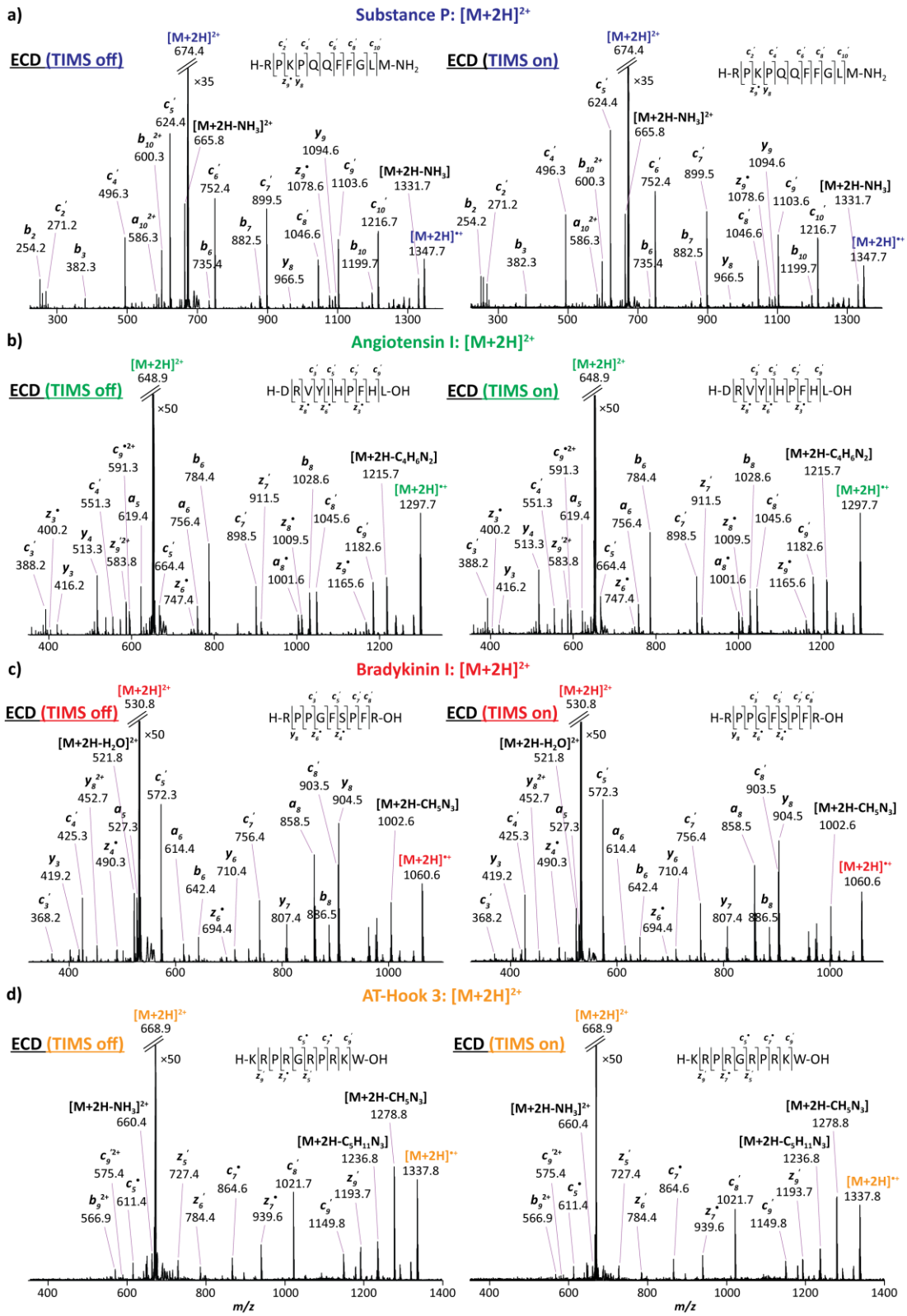

Figure S8. ECD spectra of the $[M + 2H]^{2+}$ ions of (a) substance P, (b) angiotensin I, (c) bradykinin and (d) AT-Hook 3 when TIMS operations is off (left panel) and on (right panel).

Table S2. ECD efficiency yields (%) of the investigated peptides obtained in the TIMS-q-ECD-ToF MS per ion mobility band and in the FT-ICR MS platforms. Note that the efficiency yields arise from the sum of intensities (peak height) for all fragments observed in the ECD spectra.

Peptides	IMS band 1	IMS band 2	IMS band 3	FT-ICR
Substance P	10.3 ± 0.1	5.8 ± 0.1	-	6.9 ± 0.1
Angiotensin I	5.9 ± 0.1	4.2 ± 0.1	4.1 ± 0.05	3.6 ± 0.1
Bradykinin	6.6 ± 0.2	4.8 ± 0.1	3.0 ± 0.05	4.4 ± 0.1
AT-Hook 3	7.0 ± 0.3	4.6 ± 0.3	3.2 ± 0.42	18.9 ± 0.7

REFERENCES

1 N. A. Pierson, L. Chen, D. H. Russell and D. E. Clemmer, *J. Am. Chem. Soc.*, 2013, **135**, 3186-3192.

2 N. A. Pierson, L. Chen, S. J. Valentine, D. H. Russell and D. E. Clemmer, *J. Am. Chem. Soc.*, 2011, **133**, 13810-13813.